First astrometric reduction of Cassini ISS images using an automatic procedure: application to Enceladus images 2013-2017

Q. F. Zhang,[1,5]* V. Lainey,[2,4] N. J. Cooper[3,4] A. Vienne[4,5] Q. Y. Peng[1,5] and Y. T. Xiong[1]

[1]*Department of Computer Science, Jinan University, Guangzhou 510632, P. R. China*
[2]*Jet Propulsion Laboratory, California Institute of Technology, 4800 Oak Grove Drive, Pasadena, CA 91109-8099, United States*
[3]*Astronomy Unit, School of Physics & Astronomy, Queen Mary University of London, Mile End Road, London, E1 4NS, UK*
[4]*IMCCE, Observatoire de Paris, UMR 8028 du CNRS, UPMC, Université de Lille 1, 77 av. Denfert-Rochereau, 75014 Paris, France*
[5]*Sino-French Joint Laboratory for Astrometry, Dynamics and Space Science, Jinan University, Guangzhou, 510632, P. R. China*

ABSTRACT

We provide new astrometric observations of Enceladus from images taken using the *Cassini* Imaging Science Subsystem (ISS) Narrow Angle Camera. Astrometric reduction was performed using a new fully-automatic camera repointing technique built within the *Caviar* software package. The new automatic procedure is based on the *k-d tree* technique, and has been developed as an alternative to the manual technique currently available in *Caviar*. We describe the new procedure and demonstrate its effectiveness compared to manual processing. Repointing corrections were computed using reference stars from the UCAC4 and Gaia DR1 star catalogues. We compare the observed-minus-computed (O-C) residuals of Enceladus based on UCAC4 with those based on Gaia DR1, relative to the JPL SAT375 ephemeris and the IMCCE NOE ephemeris, respectively. We reduced all available Cassini ISS images of Enceladus during the period 2013-2017, producing a total of 1109 Cassini-centered astrometric observation. These are provided in right ascension (α) and declination (δ) in the International Celestial Reference Frame (ICRF). Estimated mean O-C residuals relative to JPL's SAT375 ephemeris were 0.7 km in $\alpha*\cos(\delta)$ and 1.8 km in δ, with standard deviations of 2.4 km and 3.2 km, respectively. No improvement in the precision of the observations was obtained when using the GAIA DR1 star catalogue compared to UCAC4.

Key words: astrometry –planets and satellites: individual: Enceladus – methods: observational – catalogs

1 INTRODUCTION

Images from the *Cassini* Imaging Science Subsystem (ISS) have routinely been used to measure the astrometric positions of planetary satellites throughout the duration of the *Cassini* mission. Cooper et al. (2006) reduced ISS images of the inner Jovian satellites, Amalthea and Thebe from Cassini's Jupiter flyby. Spitale et al. (2006) provided ISS astrometric observations of several small inner Saturnian satellites and improved their orbits. Cooper et al. (2008) described the discovery, astrometry and dynamics of a new Saturnian satellite, Anthe. Tajeddine et al. (2013, 2015) reduced observations of the main Saturnian satellites, Mimas, Enceladus, Tethys, Dione, Rhea, Iapetus and Phoebe from ISS images. In addition, Desmars et al. (2013) reduced ISS images of Phoebe in combination with other existing space-based and ground-based observations, demonstrating that the availability of *Cassini* ISS observations was a crucial factor in being able to improve the accuracy of the orbit of Phoebe. Cooper et al. (2014) presented astrometric

observations of the Saturnian satellites Mimas, Enceladus, Tethys, Dione, and Rhea from ISS images of mutual occultations between these satellites, allowing inter-satellite separations of high accuracy to be generated due to the cancellation of camera pointing errors for measurements made in the same image. Cooper et al. (2015) performed ISS astrometry of the small inner Saturnian satellites, Atlas, Prometheus, Pandora, Janus and Epimetheus, improving the precision of their orbits and masses, and additionally showing that the motion of Atlas is chaotic, as a result of a resonant interaction with Prometheus. All of the above examples have demonstrated that the high accuracy can be obtained from the astrometric reduction of Cassini ISS images.

The Saturnian satellite Enceladus has been a subject of particular interest following the discovery of geysers, an icy outer shell and liquid layer beneath it (Porco et al. 2006; Thomas et al. 2016), and astrometric methods have been shown to play a key role in solving the fundamental problems relating to the structure and dynamical evolution of Enceladus and the Saturnian satellite system as a whole (Lainey et al. 2012; Thomas et al. 2016; Lainey et al. 2017).

---

* E-mail: tqfz@jnu.edu.cn

In addition to making available Cassini ISS astrometric observations of Enceladus from 2013 to 2017, the aims of this paper are (1) to investigate the feasibility of performing fully automatic astrometry within the framework of the *Caviar* software package, and (2) to evaluate the benefits, if any, of using the Gaia DR1 reference star catalogue in the astrometric reduction, compared to the UCAC4 catalogue. The astrometric reduction method is described in Section 2. The observations and analysis are given in Section 3. We conclude in Section 4.

2   ASTROMETRY

Methods for the astrometric reduction of Cassini ISS images using proprietary software have been described in Cooper et al. (2006, 2008) and Tajeddine et al. (2013). The development of these methods over the course of the Cassini mission culminated in the release to the community of the *Caviar* software package, developed jointly by QMUL (Queen Mary University of London) and IMCCE (Institut de mécanique céleste et de calcul des éphémérides)(Cooper et al. 2018). In *Caviar*, the astrometric data reduction pipeline includes two main steps: a correction for errors in the nominal spacecraft camera pointing direction, followed by the astrometric measurement of the centre of the target planetary satellite. In the first step, the correction to the camera pointing direction is estimated by matching reference stars from a star catalogue (currently UCAC4) with imaged stars. In the second step, the position of the centre of the target satellite is measured using either limb-fitting or centroiding, depending on whether or not the target satellite is resolved in the image.

At present, the Caviar package has no capability for the automatic correction of the camera pointing direction (Cooper et al. 2018). Currently a 'bulk' manual alignment step is required in order to achieve an approximate match between the catalogue and imaged star positions before a final statistical fit is performed. Hence, the only barrier to fully-automatic repointing has been the development of a satisfactory technique to allow the 'bulk' star alignment to be performed fully automatically, removing the need for any manual intervention. Considering the potentially large number of images to be reduced for a given target satellite, including possibly non-clear filter images with stars in the background, and the difficulty of matching stars in some cases, we think that the automatic pointing correction is a necessary upgrade. Cooper (2004) developed a solution based on automatic 2-dimensional cross-correlation in the wavenumber domain, using fast-fourier transforms. Although efficient, the method lacked robustness in the presence of noise, requiring some image pre-enhancement. Here we have developed an entirely new fully-automatic repointing method based on k-d tree (Bentley 1975). In the following we provide a detailed description of this technique.

2.1   Fully-automatic repointing based on k-d tree

The k-d tree, or k-dimensional tree method, is a classic space-partitioning data-structure for storage and searching (Bentley 1975). It is a binary tree in which each node is a point in a space with k dimensions. It partitions the data recursively along the dimension of maximum variance. At each iteration the variance of each dimension is computed and the data is split into two parts along the dimension of maximum variance. That is, all points with a smaller value are placed in the left sub-tree and the larger points in the right sub-tree until the last trees are only composed of one

point. This makes it particularly useful for range and nearest neighbor searches.

The k-nearest neighbors (k-NN) algorithm is a type of non-parametric method in pattern recognition (Altman 1992). Given a query point X and set S with n points, the k-NN algorithm is a solution to find the k nearest neighbors of X from S. It is well known that the search can be done efficiently by using the k-d tree in low-dimension space. Its time complexity is $o(log(n))$ (Friedman et al. 1977). When a maximal distance (threshold t) is given to limit the search range, this is referred to as ranged search. For simplicity's sake, we refer to the retrieval of the k NN with a given maximal distance t based on kd-tree as a (k,t)-NN search. The parameter k bounds the number of the nearest points and t bounds the distance. Obviously, a (k,t)-NN search has the same efficiency as k-NN search with k-d tree. Even in some cases, it has a better performance because some searching loops can be stopped when the distance exceeds the threshold t.

As mentioned above, the key to fully-automatic repointing is the ability to locate and identify reference stars automatically. We therefore propose to apply the (k,t)-NN search method for this, where k is the upper limit of the searching number of the nearest neighbors, and t is the upper limit of searching distance. Before finding reference stars, we can obtain one set of estimated coordinates that are the catalogue stars' positions in the image and one set of observed coordinates that are positions of the stars detected in the image. In the case of Cassini ISS images, the two sets of coordinates differ only in terms of an unknown translation and rotation. In practice, the rotation is very small, and can be computed in the subsequent residual correction phase. That is, the rotation can be ignored when we estimate the translation.
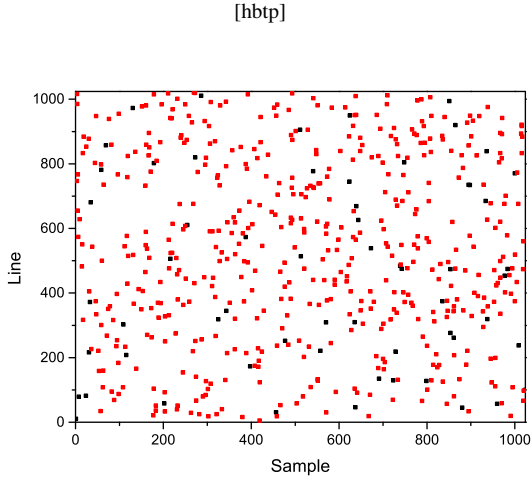
Let the estimated coordinates be one set E of m points, and the observed coordinates be one set O of n points. In the application considered here, finding reference stars means searching for the best translation from the set E to O in order to obtain the maximum number of overlay points.

The automatic finding of reference stars is then implemented using the following steps:
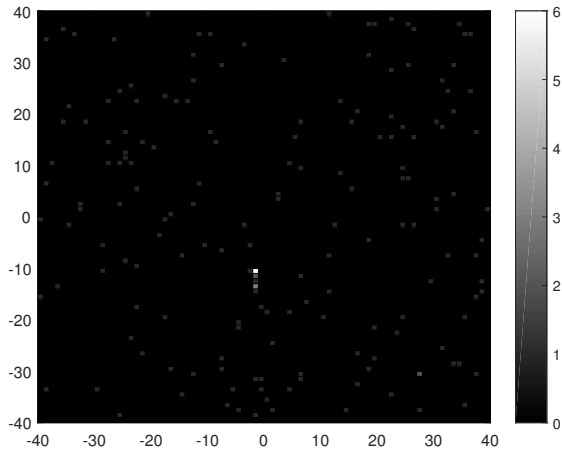
-First, store the set E by a k-d tree structure. Here, one 2D-tree structure can be used to save all the points in set E. This will speed up the following NN search.

-Second, search (k,t)-NNs for every point in set O. That is, take every point in set O as a query point, and use the k-NN search with the k-d tree algorithm to look up all the nearest neighbours satisfying the constraints in number and distance. In practice, $k = 10$ and $t = 40.0$ are good enough for most of the images. In other words, we restrict the searching to finding up to 10 nearest stars within 40 pixels' distance of a query point. In extreme cases involving a very large translation (i.e. a pointing error of perhaps hundreds of pixels), k and t can be increased as required. At the same time, the nearest distance between every NN and its corresponding query point are saved into one array.

-Third, make a histogram of these nearest distances and find out its maximum. All the nearest distances cover a 2D space. We can divide the space into a grid in which every cell is $1 pixel$ by $1 pixel$, and make a 2D histogram of all these nearest distances over the grid. From the histogram, the peak can be located: the coordinate of the peak's location indicates the translation in the x and y direction. At the same time, we can find all nearest neighbours (in set E) and their corresponding query point (in set O) in the cell where the peak is located. All these pairs of NN (catalogue stars) and query points (image stars) compose the matching pairs of reference stars.

[hbtp]

(a) An example of distribution of catalogue stars and image stars in one image. The red squares are catalogue stars, the black squares are image stars.

(b) The 2D histogram of distances between them.

Figure 1. An example of catalogue stars and image stars and their distance histogram.

Table 1. Mean values (Mean) and standard deviations (SD) of residuals of all of 551 observed positions relative to the JPL SAT375 ephemeris in sample and line (in pixels).

		MEAN	SD
Automatic Method	sample	0.036	0.340
	line	0.367	0.405
Tajeddine et al 2013	sample	0.011	0.480
	line	0.964	0.533

overlay points, and the overlay points in the peak cell are directly the matching pairs of reference stars. Of course, theoretically, it is possible that the value is not equal to the number of overlay points. However, the resolution of the grid is so fine ($1\,pixel$ x $1\,pixel$) that it ensures that the overlay points are in one-to-one correspondence and prevents the possibility of one-to-many correspondences for the Cassini ISS images.

The time complexity of the whole automatic method is $o(NlogN)$, where $N = max(m,n)$. In practice, the time cost is about one tenth of a second CPU time on a 2.6GHz i7 PC.

Moreover, the algorithm can provide additional information. If the peak value is 1, there exists at most one reference star in the image. Here, the user should pick reference stars by hand, if they exist. Generally, the bigger the peak value, the more credible the reference stars.

2.2 Test of the automatic method

In order to check the performance and viability of the automatic method, we used it to reduce all 920 images of Enceladus previously reduced manually by Tajeddine et al. (2013). Of these 920 images, 551 images were successfully processed using the new method. We compare the (O-C) residuals relative to the JPL SAT375 ephemeris obtained from the new method against those from Tajeddine et al. (2013) in Figure 2, while Table 1 lists the mean values and standard deviations. From the figure and table, it can be seen that the automatic method can provide better results for astrometry. In particular, there is an obvious improvement in the line direction, showing a reduction in the (O-C) residuals compared to the manual method.

On the other hand, only 551 of 920 images could be reduced using the automatic method, representing a success rate of about 60%. This reflects some limitations with the method as it is currently implemented: generally it cannot process images with a fewer than 3 reference stars, and additionally, it does not currently take into account the quality of reference stars in its selection process. For example, if an image has only 1 or 2 reference stars, there can be many possible matches between these stars and the actual imaged stars. In such a situatiuon, we have found that, in the absence of a magnitude/quality constraint, the automatic method can make a sub-optimal choice in the selection process. Clearly it will be necessary in future to refine the technique by taking into account the star magnitude and quality, and this will be the subject of further work.

However, we should also mention in connection with this issue, that the success rate is not fixed. As pointed out by Tajeddine et al. (2013), the number of available reference stars decreases with increasing size of the target satellite, in this case Enceladus, in an image i.e. close-up images will provide fewer reference stars and the success rate will increase with the increasing distance between camera and target.
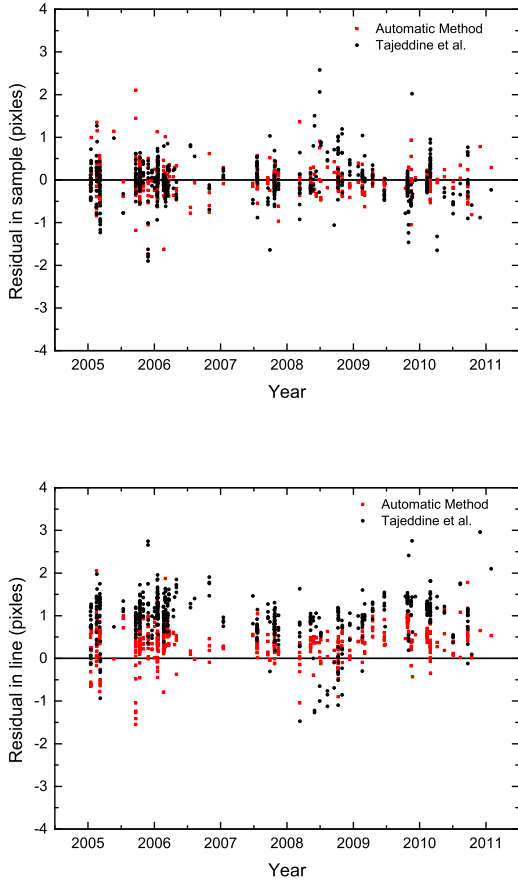
Figure 1 shows an example of histogram of distances. Fig 1(a) shows the distribution of catalogue stars and detected stars in one image, where the red squares are the detected stars, and the black squares are the catalogue stars. Fig 1(b) displays the 2D histogram of their distances in which only the distances within 40 pixels are shown and the larger distances are ignored. The grey levels indicate the number of matching pair of catalogue and image stars. The brighter is the grey, the bigger is the number. There is one white dot at (-2, -11), corresponding to the brightest dot in the histogram, which represents the maximum matching number, that is six. That means that there are six matching pairs of catalogue stars and image stars or in other words, six catalogue stars will nearly coincide with the image stars after a translation of (2, 11) pixels.

The main idea of the automatic method is to list all the possible translations in the 2D distance space. The parameters k and t dramatically reduce the range of distance space. In step 3, the histogram shows the votes for every translation. So the histogram peak gives rich information: its location presents the translation that brings the most overlay points, its value indicates the number of

Figure 2. Residuals for all 551 observed positions of Enceladus relative to SAT375 ephemeris in sample and line, respectively. The red dots represent the residuals from automatic method, and the black dots from Tajeddine et al. (2013)

3 OBSERVATION AND ANALYSIS

Astrometric reduction of pre-2013 ISS images of Enceladus was undertaken by Tajeddine et al. (2013). Here we extend the image timespan to 2017. A total number of 1109 new astrometric positions of Enceladus are reduced. Table 2 provides a sample of the complete set of reduced observations.

Following, for example Cooper et al. (2018); Tajeddine et al. (2013), the satellite positions in pixel coordinates and the camera pointing information in terms of the right ascension, declination (α_c, δ_c) and twist angle θ are provided separately. This provides the user with the flexibility to be able to re-estimate the camera pointing correction at some later date, without having to re-measure the satellite positions, and vice versa for the satellite positions.

In addition, Figure 3 shows a sample of the ISS images of Enceladus used in this work. Observation residuals relative to the JPL ephemeris SAT375 are shown in Figure 4, where the residuals in $\alpha*\cos(\delta)$ and δ have been converted to kilometres. Figure 4, shows that there is no data coverage in 2014 : the few ISS images of Enceladus taken in 2014 were not suitable for astrometric reduction. Table 3 lists the corresponding mean and standard deviation values for the residuals (in pixels, arcseconds and kilometres respectively).
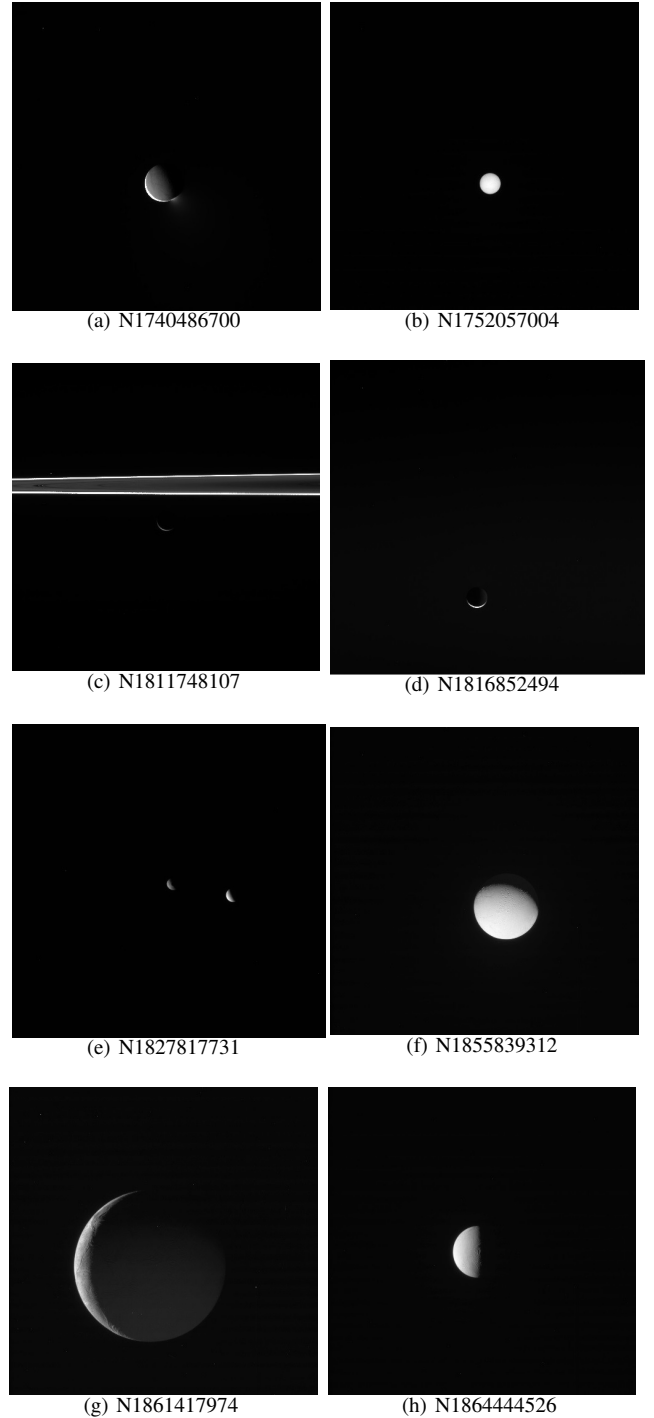

(a) N1740486700

(b) N1752057004

(c) N1811748107

(d) N1816852494

(e) N1827817731

(f) N1855839312

(g) N1861417974

(h) N1864444526

Figure 3. Some typical examples of ISS images of Enceladus reduced in this work, giving an indication of the range in resolution. Image numbers are labelled. Figure (e) contains two satellites: the larger object is Enceladus.

As mentioned above, catalogue stars are used to correct the camera's pointing, so the precision of the catalogue will affect the result of astrometry. Following the release of Gaia DR1, with its expected improvement in precision, we consider whether this provides benefits for the astrometric reduction of ISS images. We therefore compared the effects of using Gaia DR1 with the UCAC4 catalogue. For this comparison, a total of 352 ISS images from

[htbp]

Table 2. A sample of the results given by the astrometric reduction, showing: image name, date and exposure mid-time of the image (UTC), satellite name, right ascension and declination of the satellite (in the ICRF), right ascension and declination of the camera pointing vector, twist angle (defined in Tajeddine et al. (2013), sample and line (in pixels) of the observed satellite in the image, and finally the number of the reference stars in the image. All the angle variables are given in degrees.

Image name	Mid-time (UTC)	Body	α (degrees)	δ (degrees)	α_c (degrees)	δ_c (degrees)	Twist angle (degrees)	Sample (pixels)	Line (pixels)	Stars
N1751142896	2013-179T19:39:19.633	ENCELADUS	243.112610	8.961039	243.105022	8.953827	235.917140	481.84	517.86	6
N1752052262	2013-190T08:15:19.709	ENCELADUS	212.517539	-13.404226	212.547617	-13.409896	91.050946	529.57	596.36	3
N1811748107	2015-151T06:19:44.727	ENCELADUS	75.190815	-5.020491	75.191262	-5.022992	3.992708	510.70	518.86	17
N1812956192	2015-165T05:54:22.292	ENCELADUS	139.522300	1.373191	139.518650	1.370494	6.344389	522.97	518.13	8
N1816843209	2015-210T05:37:30.953	ENCELADUS	64.349043	-5.553346	64.363040	-5.642869	2.688098	483.19	773.91	11
N1820590327	2015-253T14:29:07.118	ENCELADUS	81.380429	-4.624617	81.380598	-4.714882	4.304750	530.73	773.75	21
N1827866095	2015-337T19:31:09.514	ENCELADUS	144.177472	1.028904	144.167798	1.024324	5.055270	540.78	522.30	3
N1836392609	2016-071T11:58:46.225	ENCELADUS	84.146578	-1.232567	84.014959	-1.225681	4.533781	892.01	461.19	6
N1855838952	2016-296T13:42:27.228	ENCELADUS	214.311083	-61.194273	214.368331	-61.199160	107.869347	549.09	583.17	2
N1859559854	2016-339T15:17:05.597	ENCELADUS	263.590485	29.841252	263.585604	29.847040	265.228851	527.27	525.24	2
N1861418172	2016-361T03:28:51.455	ENCELADUS	116.127862	43.755468	116.177495	43.753098	23.002871	418.13	558.68	3
N1864085102	2017-026T00:17:21.855	ENCELADUS	91.636928	-1.050486	91.633832	-1.143753	5.113481	544.75	781.31	32
N1867761637	2017-068T13:32:34.218	ENCELADUS	83.110276	3.937462	83.119645	3.846899	4.496720	505.04	776.64	35
N1869659477	2017-090T12:43:00.275	ENCELADUS	86.693833	-1.836697	86.706708	-1.929274	4.745260	496.45	783.37	14

2015 were each reduced using UCAC4 (Zacharias et al. 2013) and Gaia DR1 (Gaia Collaboration 2016a,b) respectively.

For each image, we select the same reference stars from Gaia DR1 and UCAC4, then correct the pointing. We limit the maximum magnitude of reference stars to be 14, since the ISS NAC's limiting magnitude is 14 in 1 s through the clear filter (Porco et al. 2004). Moreover, fainter stars tend to be unsuitable for position measurement, even if the exposure time is extended and a different filter is used (longer exposures can cause smearing). Generally, under the restriction of a maximum magnitude of 14, the set of candidate stars from Gaia DR1 is the same from UCAC4 in the same field of view, while in a few cases, Gaia can provide a little more candidate stars than UCAC4. In these situations, we take the common stars in Gaia and UCAC4 as reference stars.

Hence, we get two corrected pointing directions, one derived from UCAC4, and the other from Gaia DR1. Considering Gaia DR1 has no proper motion information for most stars, we selected only the images in 2015 and ignored their proper motions when using Gaia reference stars. After correcting the pointing, we measure the position (sample and line) of Enceladus in an image, then reduce, to give the corresponding position of Enceladus in the ICRF using each of the two different corrected pointing directions. That is, each image is reduced twice under one specific ephemeris, and has two results relative to the ephemeris, one from Gaia DR1, and the other from UCAC4. Finally, we compare the result pairs of total 352 images to analyze the effects brought by two catalogues.

Figure 5 shows the results from UCAC4 and Gaia DR1 relative to the JPL SAT375 ephemeris. Figure 5(a) shows the residuals of 352 observations relative to the SAT375 in sample and line when using Gaia DR1 to correct the camera's pointing direction. Black dots indicate the residuals in the sample direction, and the red dots in the line direction. Units are pixels. Figure 5(b) shows the corresponding residuals when the pointing is corrected using UCAC4. Figure 5(c) shows the difference between the residuals in (a) and (b). Evidently the differences are small. Figure 6 is the same as Figure 5 except with the residuals computed relative to the IMCCE NOE ephemeris. The Table 4 lists the mean values and standard deviations of the two sets of residuals relative to the two different ephemerides (SAT375 and NOE). Comparing Figure 5(c) and Figure 6(c), it is clear that the differences are very small. The mean and standard deviation of (o-c)$_{gaia}$-(o-c)$_{ucac4}$ in Table 4 also support this. From these results, we conclude that there is no improvement in precision or accuracy when using Gaia DR1 compared to UCAC4 for the correction of the pointing of Cassini ISS images. This is largely to be expected because the errors in the astrometric reduction are dominated by errors from a variety of sources, all of

Table 3. Mean values (Mean) and standard deviations (SD) of residuals of all of 1109 observed positions relative to the JPL SAT375 ephemeris, which presented in pixels, arcseconds and kilometers respectively.

|	Mean	SD
Sample (pixel)	0.052	0.382
Line (pixel)	0.197	0.479
$\alpha*\cos\delta$ (arcsec)	0.098	0.573
δ (arcsec)	0.270	0.590
$\alpha*\cos\delta$ (km)	0.698	2.378
δ (km)	1.830	3.220

which far exceed the precision of GAIA DR1: for example, the random error in measurement, the error in limb fitting and error from non-zero solar phase angles. The latter alone can produce a significant systematic bias of the order of 0.5 pixel (Cooper et al. 2014). Even if the phase bias can be removed by some other technique (for example, theoretical computation, or statistic modelling of images with similar phase), it would be difficult to approach the level of precision of Gaia DR1. Other biases also contribute to the total error, for example, the errors from edge detection, the error resulting from the fitting of the projection of the target satellite's ellipsoid to the detected edge, and the error of the target's shape. Currently all of these errors significantly exceed the precision of Gaia DR1 : the challenge moving forward will be to reduce these errors in order to take advantage of the potential benefits in precision that the Gaia catalogue can provide. Although in this particular case, we did not see an improvement in sky coverage using Gaia DR1 compared to UCAC4, in a more general sense, given the much higher density coverage in Gaia overall, that may be the only benefit in the short term that we can expect from Gaia for this type of work, until the astrometric measurement techniques themselves can be improved.
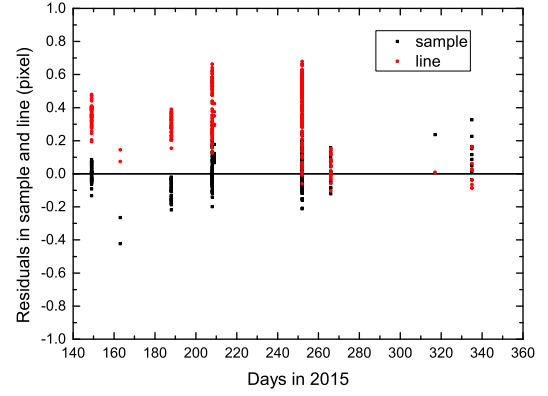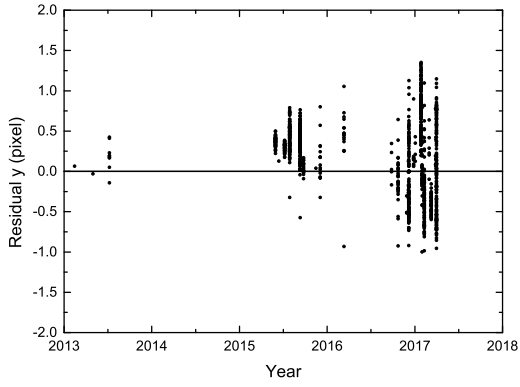
4 CONCLUSIONS

We describe a new fully-automatic repointing method that uses (k,t)-NN search algorithm with KD-Tree. A comparison of the results from the auto procedure with those from Tajeddine et al. (2013) illustrates its effectiveness for the reduction of Cassini ISS images.

A total of 1109 ISS images of Enceladus in 2013-2017 are reduced. The results show that their mean residuals relative to JPL SAT375 are 0.7 km in $\alpha*\cos(\delta)$ and 1.8 km in δ, with standard deviations of 2.4 km and 3.2 km respectively.
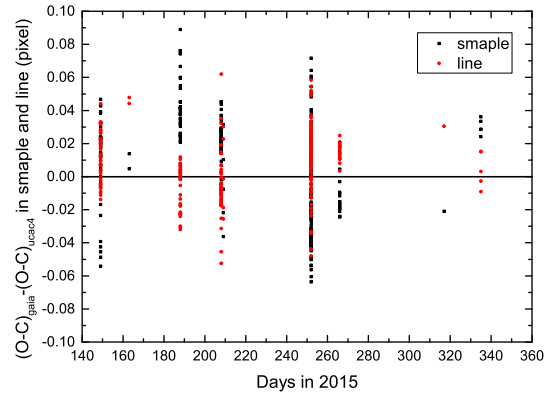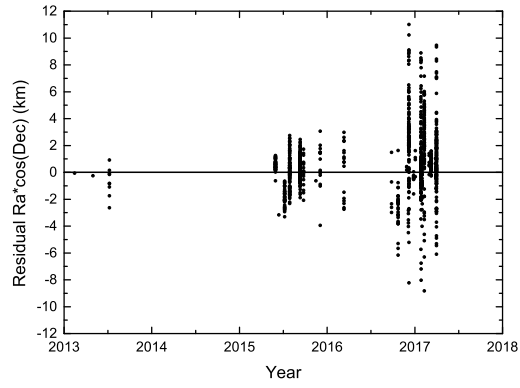
Comparing the results of 352 ISS images of Enceladus in 2015 when the reference stars are from Gaia DR1 and UCAC4 respec-
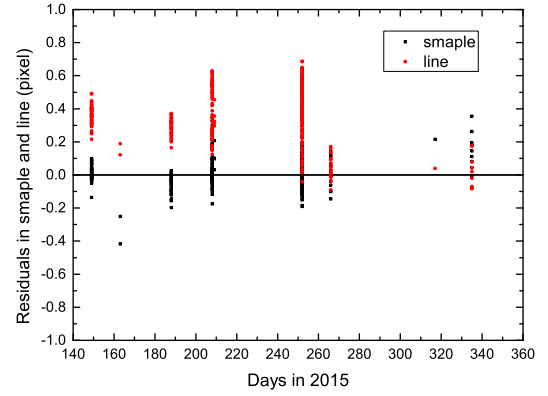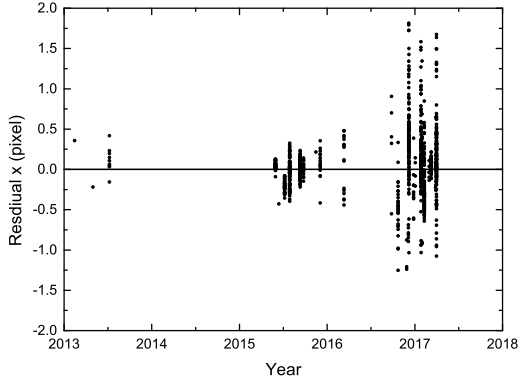
(a) (O-C)s relative to SAT375 under the pointing from Gaia DR1

(b) (O-C)s relative to SAT375 under the pointing from UCAC4

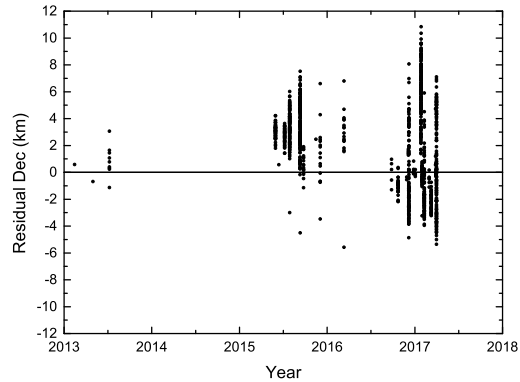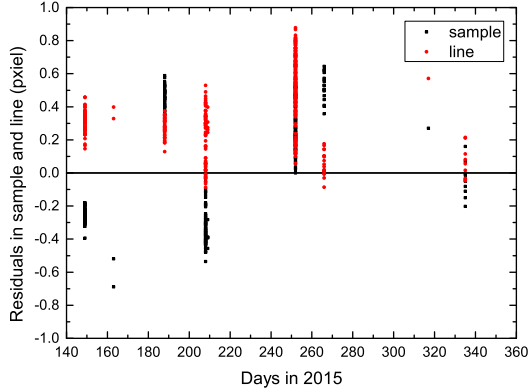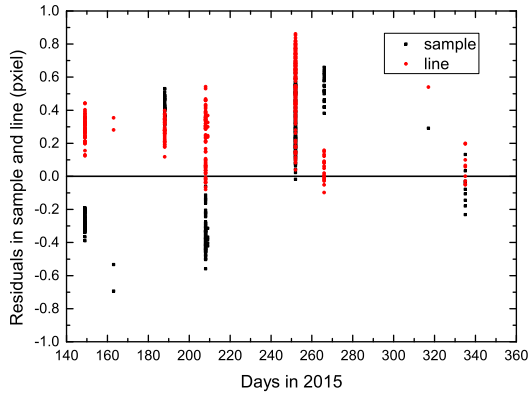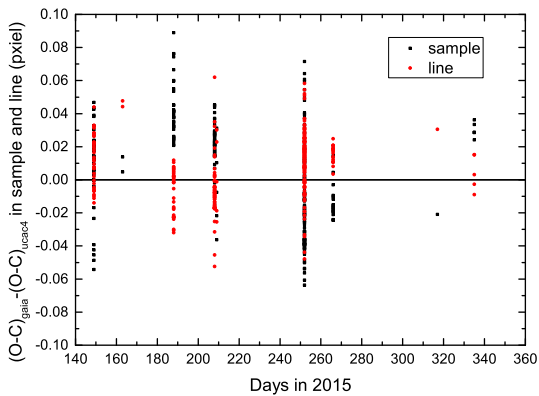(c) Difference between the above residuals

Figure 5. O-C residuals relative to JPL'S SAT375 ephemeris, comparing the results of repointing using UCAC4 or Gaia DR1. (a) The residuals for 352 observed positions of Enceladus in 2015 relative to the SAT375 ephemeris in sample and line respectively. For each observed position, the camera's pointing is corrected using Gaia DR1. (b) The same residuals but pointing corrected using UCAC4. (c) The difference between the two kinds of residuals in sample and line respectively.

Figure 4. Residuals for all 1109 observed positions of Enceladus relative to SAT375 ephemeris in x (sample) , y (line), $\alpha*\cos(\delta)$ and δ respectively. Note: the residuals are converted to kilometers in each direction.

(a) (O-C) residuals relative to the IMCCE NOE ephemeris, using pointing based on Gaia DR1

(b) (O-C) residuals relative to the IMCCE NOE ephemeris, using pointing from UCAC4

(c) Difference between the above residuals

Figure 6. O-C residuals relative to the IMCCE NOES ephemeris, comparing the results of repointing using UCAC4 or Gaia DR1. (a) The residuals for 352 observed positions of Enceladus in 2015 relative to the NOE ephemeris in sample and line respectively. For each observed position, the camera's pointing is corrected by Gaia DR1. (b) The same residuals but pointing corrected by UCAC4. (c) The difference between two kinds of residuals in sample and line respectively.

Table 4. Mean values of (O-C)s in pixels relative to the JPL SAT375 ephemeris and NOE ephemeris respectively, including standard deviations, when the Gaia DR1 and UCAC4 are used to obtain Enceladus' positions respectively.

			MEAN	**SD**
SAT375	Ucac4	sample	0.012	0.100
		line	0.349	0.170
	Gaia	sample	0.017	0.094
		line	0.356	0.166
	(o-c)$_{gaia}$-(o-c)$_{ucac4}$	sample	0.005	0.030
		line	0.006	0.018
NOE	Ucac4	sample	0.101	0.365
		line	0.368	0.227
	Gaia	sample	0.106	0.356
		line	0.374	0.229
	(o-c)$_{gaia}$-(o-c)$_{ucac4}$	sample	0.005	0.030
		line	0.006	0.018

tively, we find the two catalogues bring nearly equivalent precision of reduction.

References

Altman N. S. 1992, The American Statistician, 46(3), 175
Bentley J. L. 1975, Comm. ACM, 18, 509
Cooper N. J. 2004, PhD Thesis, University of London
Cooper N. J., Murray C. D., Porco C. C., & Spitale J. N. 2006, Icarus, 181, 223
Cooper N. J., Murray C. D., Beurle K., et al. 2008, Icarus, 195, 765
Cooper N. J., Murray C. D., Lainey V., Tajeddine R., Evans M. W., & Williams G. A. 2014, A&A, 572, A43
Cooper N. J., Renner S., Murray C. D., & Evans M. W. 2015, AJ, 149, 27
Cooper N. J., Lainey V., Meunier L. E., et al. 2018. A&A, 610, A2
Desmars J., Li S. N., Tajeddine R., et al. 2013, A&A, 553, A36
Friedman J. H., Bently J., and Finkel R. A. 1977, ACM Transactions on Mathematical Software, 3, 209
Gaia Collaboration, Prusti T., Bruijne J. H., et al. 2016a, A&A, 595, A1
Gaia Collaboration, Brown A. G., Vallenari A., et al. 2016b, A&A, 595, A2
Lainey V., Arlot J.-E., Karatekin O., & van Hoolst, T. 2009, Natur, 459, 957
Lainey V., Karatekin O., Desmars J., et al. 2012, ApJ, 752, 14
Lainey V., Jacobson R. A., Tajeddine R., et al. 2017, Icar, 281,286
Porco C. C., West R. A, Squyres S., et al. 2004, SSRv, 115, 363

Porco C. C., Helfenstein P., Thomas P. C., et al. 2006, Sci, 311, 1393

Spitale J. N., Jacobson R. J., Porco C. P., & Owen W. M. 2006, AJ, 132, 692

Tajeddine R., Cooper N. J., Lainey V., Charnoz S., & Murray C. D. 2013, A&A, 551, A129

Tajeddine R., Lainey V., Cooper N. J., & Murray C. D. 2015, A&A, 575, A73

Thomas P. C., Tajeddine R., Tiscareno M. S., et al. 2016, Icar 264, 37

Zacharias N., Finch C. T., Girard T. M., et al. 2013, AJ, 145, 44

This paper has been typeset from a TEX/LATEX file prepared by the author.